J. Fluid Mech. (1996), *vol.* 329, *pp.* 1–24

Experimental studies of a distorted turbulent spot in a three-dimensional flow

By M. JAHANMIRI[1],† A. PRABHU[1] AND R. NARASIMHA[1,2]

[1]Department of Aerospace Engineering, Indian Institute of Science, Bangalore 560 012, India

[2]The Jawaharlal Nehru Centre for Advanced Scientific Research, Bangalore, India

(Received 28 November 1994 and in revised form 4 April 1996)

We report here on the results of a series of experiments carried out on a turbulent spot in a distorted duct to study the effects of a divergence with straight streamlines preceded by a short stretch of transverse streamline curvature, both in the absence of any pressure gradient. It is found that the distortion produces substantial asymmetry in the spot: the angles at which the spot cuts across the local streamlines are altered dramatically (in contradiction of a hypothesis commonly made in transition zone modelling), and the Tollmien–Schlichting waves that accompany the wing tips of the spot are much stronger on the outside of the bend than on the inside. However there is no strong effect on the internal structure of the spot and the eddies therein, or on such propagation characteristics as overall spread rate and the celerities of the leading and trailing edges. Both lateral streamline curvature and non-homogeneity of the laminar boundary layer into which the spot propagates are shown to be strong factors responsible for the observed asymmetry. It is concluded that these factors produce chiefly a *geometric* distortion of the coherent structure in the spot, but do not otherwise affect its dynamics in any significant way.

1. Introduction

The birth of turbulent spots may be said to mark the beginning of the transition zone in the boundary layer, so understanding of their behaviour is essential for modelling the transition zone adequately. But the structure of a spot and the manner in which an 'island' of turbulence can maintain itself or even grow as it propagates into laminar flow have been subjects of great fundamental interest as well. After the early work of Emmons (1951) and of Schubauer & Klebanoff (1955), various studies have been made in two-dimensional constant-pressure flows; a good summary of more recent work is contained in Riley & Gad-el-Hak (1985), and in a series of papers edited by F.T. Smith (1994). The basic features of the structure of a turbulent spot have been established by Wygnanski, Sokolov & Friedman (1976) and Cantwell, Coles & Dimotakis (1978), using hot-wire and laser-Doppler measurements in the plane of symmetry of a spot; Coles (1981) concludes, on the basis of this and other work, that the main feature of the structure is a single large Λ-shaped vortex with its corner under the thickest part of the spot. There has also been the suggestion that a spot may in fact contain an array of Λ vortices (Perry, Lim & Teh 1981).

† Present address: Department of Mechanical and Aerospace Engineering, University of Science and Technology, Shahin Shahr City, Isfahan, Iran.

Source	Leading edge	Trailing edge
Schubauer & Klebanoff (1955)	0.5	0.88
Wygnanski *et al.* (1976)	0.5	0.89
Cantwell *et al.* (1978)	0.59	0.87
Antonia *et al.* (1981)	0.53	0.74
Wygnanski *et al.* (1982)	0.57	0.89
Gutmark & Blackwelder (1987)	0.58	0.88
Present measurements	0.56	0.86

TABLE 1. Celerity at turbulent wedge centreline as fraction of free-stream velocity ($y = 0.1\delta_L$).

corner under the thickest part of the spot. There has also been the suggestion that a spot may in fact contain an array of Λ vortices (Perry, Lim & Teh 1981).

There have been several proposals about the mechanism underlying spot growth. Wygnanski, Haritonidis & Kaplan (1979), who discovered Tollmien-Schlichting-type waves at the wing tips of the spot, suggest that growth occurs by fresh breakdown at these waves. Gad-el-Hak, Blackwelder & Riley (1981) also attribute spot growth to destabilization of the laminar boundary layer in the vicinity of the spot. On the other hand, based on their own experiments, Chambers & Thomas (1983) concluded that the spots form not from the breakdown of wave packets arising at the spot generator but from the longitudinal structures which precede the wave packets. More recently, Gutmark & Blackwelder (1987), experimenting in a heated laminar boundary layer, suggest that the breakdown into turbulence, and hence the growth of the spot, depends on the scale and intensity of the eddies within the overhang and on the stability characteristics of the laminar boundary layer. On the celerities themselves there has been generally good agreement among the results of different experiments (see table 1).

Some experiments have been done on the effects of pressure gradient as well. Wygnanski (1981) and Katz, Seifert & Wygnanski (1990) report low spread rates in favourable pressure gradients of the Falkner–Skan type. Clark, Jones & LaGraffe (1993) find similar evidence for the inhibiting effect of favourable pressure gradients on naturally occurring spots. Narasimha, Subramanian & Badrinarayanan (1984*a*) made measurements in flows in which the free-stream velocity changes monotonically from one constant value to a higher constant value downstream. They found that the resulting spot envelope (or turbulent wedge) is not necessarily linear in general, but as pressure gradients decrease downstream the wedge grows rapidly and tends eventually to linear growth. In experiments with adverse pressure gradients, on the other hand, Gostelow & Blunden (1992) find that growth rate can double. Kohama (1988) studies the effects of longitudinal curvature.

All of these investigations have been in two-dimensional flows, and the spot always appears as a symmetrical arrow-head-shaped region with an overhang at the leading edge and a hump just behind it. There has to-date been no study of spots in three-dimensional flows. Apart from parameters like pressure gradient and longitudinal streamline curvature, lateral curvature and divergence and convergence of streamlines may also affect a given flow (e.g. swept wings and bodies, studied by Poll 1985, Kowsky & Bippes 1988 and Ahmed, Wentz & Nyenhuis 1989). It should therefore be of value in the understanding of the transition zone if the effect of these three-dimensional parameters is studied separately; it is also possible that such investigations can shed further light on spot-growth mechanisms.

In particular, streamline convergence and divergence are known to produce large

effects on turbulent boundary layer growth, and so may be expected to have similarly large effects on transition characteristics as well. While modelling the transition zone in flows with non-parallel streamlines, it is often assumed that the spot propagation envelope is inclined at a constant angle to the local streamline, the angle being therefore the same as in two-dimensional flows; this assumption goes back to the work of Emmons & Bryson (1952), and has been adopted by Chen & Thyson (1971) in their widely used transition zone model. It has been pointed out (Narasimha 1985) that this hypothesis predicts extremely rapid growth in divergent flow: if the divergence is of the radial source type, the turbulent 'wedge' swept out by the spot would be a logrithmic spiral, and its edges would come together at an azimuth 180° away from the point of spot generation. By an analysis of intermittency distributions in transitional boundary layers subjected to different favourable pressure gradients, Narasimha *et al.* (1984*a*) provided indirect evidence that the assumption may not be valid. However the hypothesis has never been directly tested.

The present experiments were thus undertaken with the specific objective of studying the structure of the turbulent spot and its characteristics in a situation where streamlines are not parallel, although the pressure gradient is zero. This is achieved by studying spots on a flat plate (measuring surface) forming one side of a distorted duct, whose constant cross-sectional area along its length ensures virtually constant pressure. Some preliminary results from this study have been briefly published elsewhere (Jahanmiri, Prabhu & Narasimha 1995).

2. Experiments

2.1. *The set-up*

The low-turbulence wind tunnel at the Department of Aerospace Engineering (nominal free-stream turbulence 0.03%) has been modified (figure 1) to provide a distorted flow under constant pressure. The modification takes the form of installing in the test section a distortion duct that has a converging top wall and a diverging sidewall, with a flat plate (which is the measuring surface) forming the bottom surface of the duct. This configuration avoids longitudinal streamline curvature, but due to the 'bend' in the diverging sidewall the flow undergoes a short stretch of lateral streamline curvature with little or no divergence, followed by a longer region in which the streamlines diverge almost radially. The distorted duct has a constant cross-sectional area all along its length, and thus the pressure gradient is virtually zero, although there could be a short and slight blip in the pressure distribution near the transition from the parallel to the diverging duct (Prabhu & Rao 1981; Saddoughi & Joubert 1991).

The measurement set-up consists of (i) an exciter for turbulent spot generation, (ii) hot wire anemometry for measurement of velocity, and (iii) a system for monitoring the turbulent signals and data acquisition and processing. These are described below.

An artificial spot is generated by driving sufficiently strong pulses of air through a 1 mm static hole on the flat plate using a 10 W Clarion make high-fidelity loudspeaker. Two locations for the spot source have been used: in what we shall call the 'main' series of experiments the source is upstream of the bend, at $x = 100$ mm and $z = 120$ mm (the coordinate system is indicated in figure 1), and in a 'subsidiary' series it is downstream of the bend, at $x = 294$ mm and $z = 130$ mm. The loudspeaker is excited by a variable-voltage (0–5 V), variable width pulse generator. The frequency of the pulse is controlled by a square wave derived from a separate low-frequency oscillator.

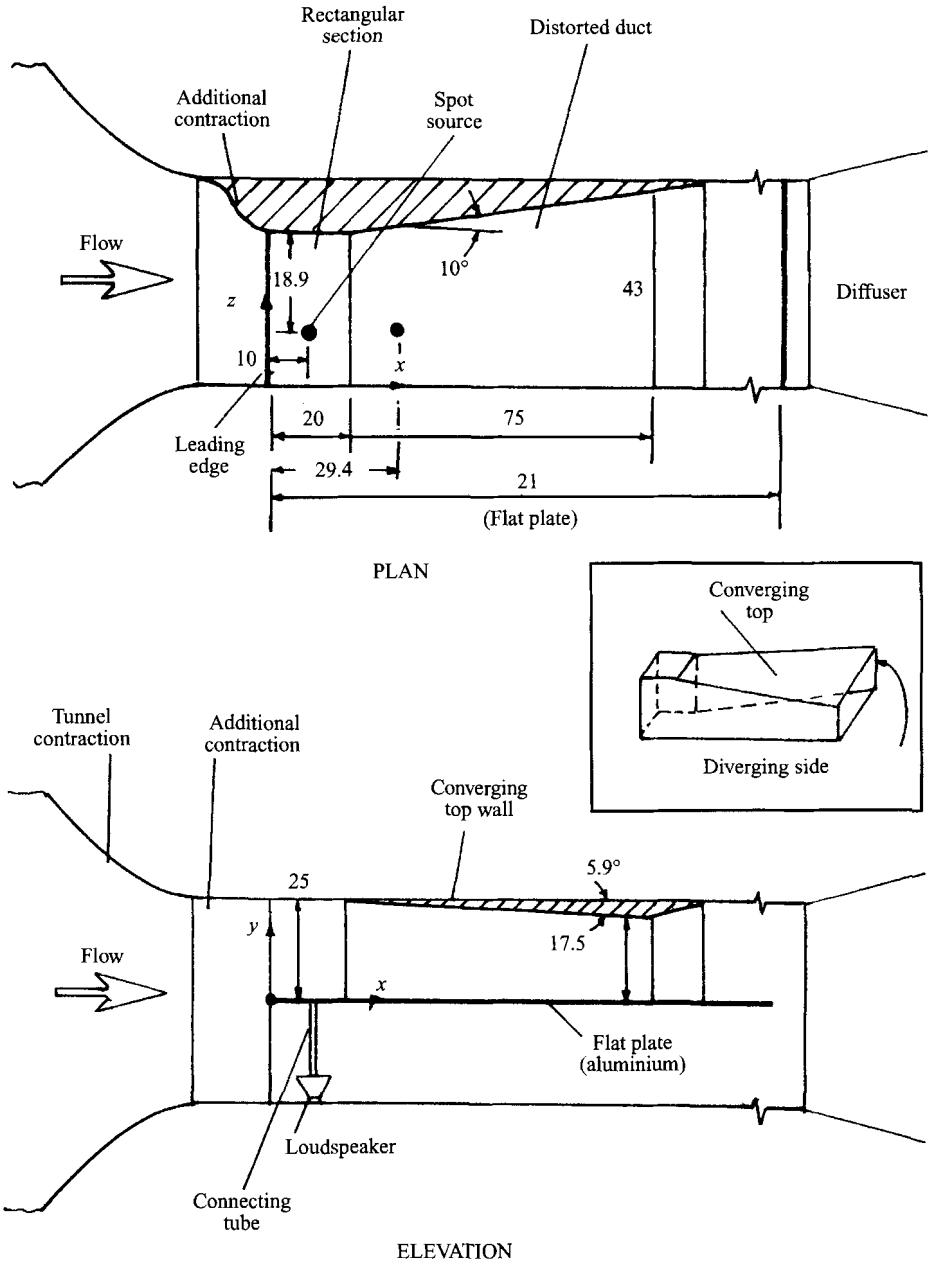

FIGURE 1. Schematic view of the experimental set-up. Inset shows an isometric view of the distorted duct (dimensions in cm).

Based on preliminary experiments, a spot generation rate of up to 3 per second was adopted in the main series of experiments, carried out at a tunnel wind speed of 10 m s^{-1}. At higher rates the wake left behind by a spot interferes with the succeeding spot at the last streamwise measurement station. In the subsidiary series, in which tunnel speed was lower (6.2 m s^{-1}), the frequency was reduced to 1 per second.

A Sunshine Industries Model No. 717 constant-temperature hot-wire anemometer system was used for making streamwise velocity measurements in the flow. A single

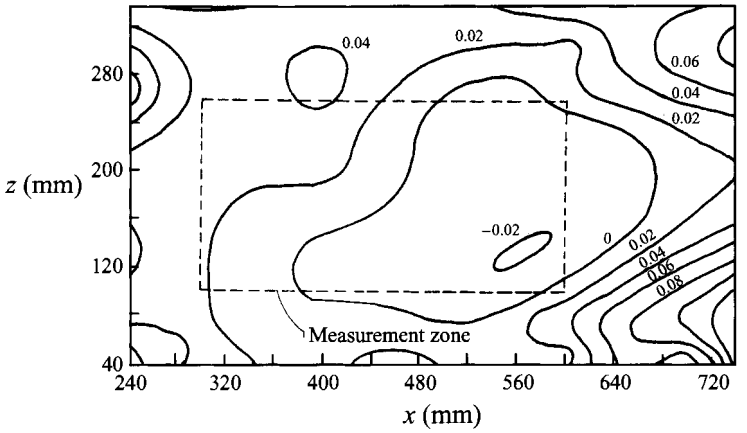

FIGURE 2. The contours of the normalized constant static pressure in the duct at $y = 1$ mm.

normal wire probe, of 12μ Pt-Rh Wollaston, was used for hot-wire measurements. The frequency response of the anemometer system with this wire was about 20 kHz.

The hot-wire signal was continuously monitored on an oscilloscope, the pulse driving the loudspeaker being used as an external trigger for synchronization of the velocity signals from the hot-wire.

A B&K Model No. 2034 dual-channel digital signal analyser allows the display of the phase-averaged signal with respect to any trigger pulse. The signal was digitized at the sampling rate of 2048 Hz. The pulse driving the loudspeaker was again used as the trigger for phase averaging. Information on the phase-averaged velocity over a selected total number of spots is normally stored in the memory of the signal analyser, but can be transferred to a PC for further analysis.

A PC-based data acquisition system which could sample 16 analog channels at a maximum through-put rate of 70 kilo-samples/s was used for acquiring the fluctuating output from the CTA and triggering the square pulse driving the loudspeaker. The data were acquired at the rate of 5K samples per second on each of the two channels – the fluctuating output of the CTA and the output of the pulse generator connected to the A/D converter card. The data are stored on 40MB cartridge tapes using a drive that was interfaced to a PC/AT.

2.2. *Flow quality*

Detailed studies were undertaken in order to ensure high quality of the flow in the distorted duct. These included measurements of the distribution of velocity and static pressure, flow visualization, and measurements of flow angles on the surface as well as at the edge of the boundary layer.

Figure 2 shows contours of constant static pressure in the duct measured using a disc probe at the height $y = 1$ mm above the flat plate. The location of the area of this pressure measurement within the duct is also shown in the figure. The pressures are normalised with respect to the average dynamic pressure in the diverging duct. The deviations of the normalised pressures are seen to be within $\pm 3\%$ in the measurement region, but the small residual pressure gradient is such as to push the flow outwards from the bend. Data at $y = 5$ mm (not shown) are very similar. The centreline velocity in the duct, measured at a height of 100 mm from the flat plate, had a maximum variation of less than 1.5% of the mean along the duct, consistent with the pressure distribution shown in figure 2.

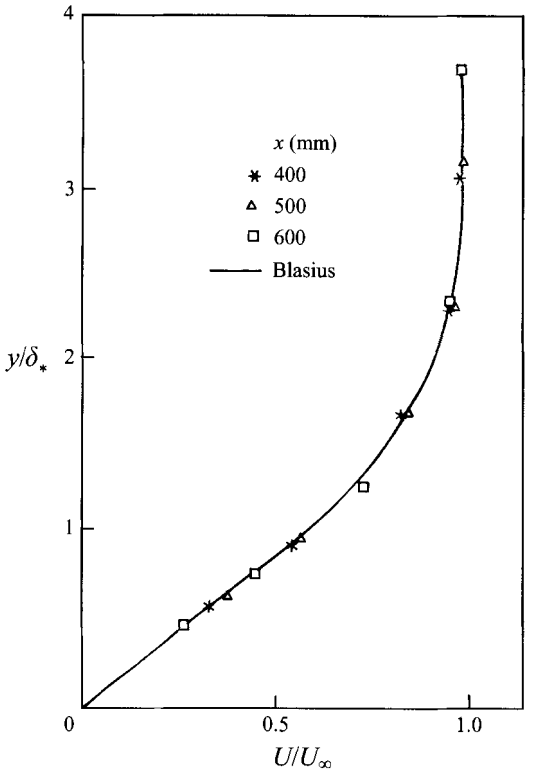

FIGURE 3. Laminar velocity profiles at different streamwise stations and $z = 0$.

Conditionally averaged velocity profiles in the laminar background flow in which the spot propagates show a similarity with the Blasius profile as demonstrated in figure 3, in agreement with the findings of Ramesh, Dey & Prabhu (1993), who also provide a theory for small flow divergence. This means that the spot is propagating in what overall is a Blasius-type profile, but there is a spanwise gradient in boundary layer thickness (higher on the outside of the bend) as shown in figure 4 which is reconstructed from figure 6 of Ramesh *et al.* (1993). This is not surprising; in any cross-flow plane the boundary layer on the outside of the bend has had a longer distance of development (i.e. 'fetch') compared to the inner side of the bend.

In the main series of experiments (tunnel speed of 10 m s^{-1} nominal), the Reynolds number based on displacement thickness δ_* at the spot source is $Re = 450$. This seemed adequate for the spot to mature early. In the subsidiary series (see §4.5) carried out at a speed of 6.2 m s^{-1}, $Re = 593$ at spot source.

Flow visualization at the surface using a mixture of lamp-black and vacuum pump oil, and tufts elsewhere, showed no separated regions inside the duct either on the sidewall or on the flat plate. Figure 5 shows the streamlines in the duct, constructed using such surface flow pictures and data from a three-hole probe traversed just beyond the edge of the boundary layer. The matching of the streamline angles between these sets is in general excellent. Flow in the boundary layer shows only very mild skewness, the maximum departure between surface and edge streamlines being less than 3°, found towards the outer edge of the bend (see figure 5). These findings are consistent with the absence of any significant pressure gradient.

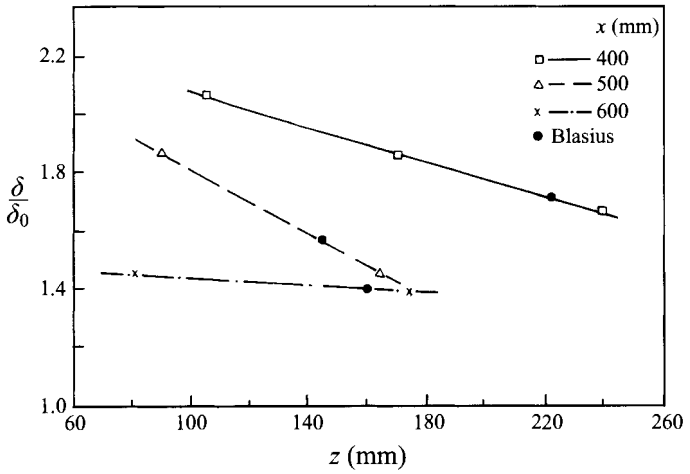

FIGURE 4. Variation of laminar boundary layer thickness in spanwise direction at different streamwise stations.

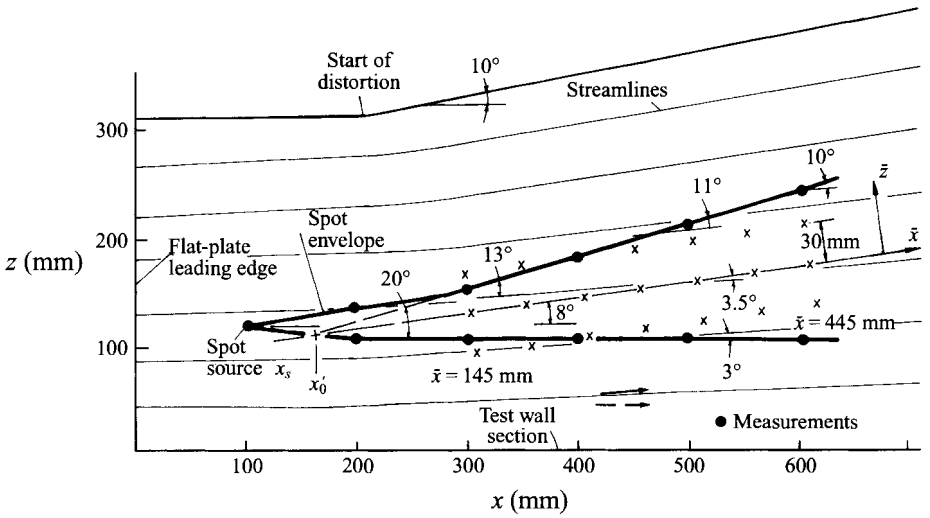

FIGURE 5. Coordinates and measurement locations. Stations with data on distribution in y are indicated by $\times$. Also spot envelope at $y = 0.5$ mm from the plate (spot source upstream of the bend).

A measure of the 'strength' of the divergence is suggested in §4.1.1.

3. Data processing technique

Various methods have been adopted for direct identification of turbulent and non-turbulent zones in any flow from velocity fluctuation data (e.g. Kovasznay, Kibens & Blackwelder 1970; Hedley & Keffer 1974; Arnal & Juillen 1977; Antonia *et al.* 1981; Kuan & Wang 1990). The technique used here (Jahanmiri, Kumar & Prabhu 1991) sensitizes the signal by squaring its double derivative, with a variable threshold depending on the noise in the laminar region of the hot-wire signal, and a variable hold time proportional to the Kolmogorov time scale. The falling edge of the pulse

driving the loudspeaker generally provides an origin for a phase time with respect to which the phases of the leading and trailing edges of the spot and the intermittency function $I(t)$ are generated.

Three different averaging procedures have been adopted in this work: (i) averaging over the turbulent or non-turbulent region based on the discrimination procedure described above, leading to 'zonal' averages (e.g. mean velocity during the passage of the spot); (ii) averaging with respect to constant phase from the falling edge of the pulse driving the loudspeaker (e.g. average time of arrival of the leading edge of a spot at a given point); (iii) averaging with respect to constant phase from the leading edge of the spot (e.g. the average velocity distribution inside a spot). The size of the ensemble for phase averaging was chosen as 100 spots; beyond 50 the phase averages do not show any appreciable changes.

4. Results and discussion

The present measurements map (for the first time in turbulent spot studies) the boundaries of the spot in fixed phase time as it propagates downstream; this is done by triggering the spot periodically and taking ensemble averages of type (ii), described in §3, over a grid of 144 points at a fixed height of 0.5 mm above the surface (in the main series of experiments), and 7 streamwise and 3 spanwise stations (with 10 points in the normal direction at each station) as shown in figure 5, involving a total of 210 measuring points. (It might at first sight seem preferable to traverse at a height proportional to the local laminar displacement thickness δ_*, but this length scale varies by about 40% from one end of the spot to the other, and is hardly relevant *within* the spot. We have preferred instead to study the spot as close to the surface as practical, and the choice of $y = 0.5$ mm reflects this requirement.) We shall use two coordinate systems for specifying location: the x, z system, aligned with the approach flow ahead of the duct and normal to it, and the $\bar{x}, \bar{z}$ system, aligned with and normal to the centreline of the turbulent wedge that develops far downstream of the bend (see figure 5).

4.1. *Overall characteristics of spot*

4.1.1. *Spot envelope and celerities*

The boundary of the turbulent wedge that is the envelope of the spot along its trajectory may be determined by tracing the locus of points where the trailing and leading edges coincide on average. Once the two edges are detected separately for each spot, the average phase time for the arrival of either edge is determined at each of the 144 grid points mentioned earlier. At each of the streamwise stations chosen for detailed measurement the $\bar{z}$ locations at which the phase time for the trailing edge and leading edge coincide are determined in order to identify the envelope of the spot. The projection of the spot envelope on the plate (or rather its cross-section at $y = 0.5$ mm above it) is the line joining these points.

Figure 5, which also shows the spot envelope so determined, suggests that the envelope is a wedge in the straight duct starting from the spot source, and that the angle of this wedge is $20° \pm 0.5°$, which closely agrees with the earlier work of Schubauer & Klebanoff (i.e. 22.6°). Even though a small variation of this angle with Reynolds number can be discerned (Narasimha 1985), a good approximate value for half this wedge angle on a flat plate is 10°. It is interesting that the envelope quickly reorients to a different wedge in the distorted duct with a centreline inclined at an angle of 8° to that in the straight duct, and that the angle of the wedge in the

	2D	Spot A	Spot B
Celerity, LE	$0.88U_\infty$	$0.86U_\infty$	$0.87U_\infty$
Celerity, TE	$0.5U_\infty$	$0.56U_\infty$	$0.54U_\infty$
Angle between spot nose and wedge CL	0.0	3.5°	1.2°
Wedge angle with local streamline	11.3°	13°–3°†	11.5°–8.5°‡
Total spread angle	22.6°	20°	20°

† At $x = 300$ mm

‡ At $x = 500$ mm

TABLE 2. Characteristics of spots in two-dimensional and in distorted flow. A, spot source located upstream; B, spot source located downstream. 2D data from Schubauer & Klebanoff (1955).

distorted duct continues at 20°. A virtual origin for the wedge in the distorted duct can be identified at x_0'. It is seen that the centreline of the wedge is not along any streamline (typically there is an angle of 3.5° between them), and further that the angle that the wedge boundary makes with the local streamlines is widely different on the two sides (varying from 13° on the inside at $x = 300$ mm to only 3° on the outside at $x = 500$ mm), and changes as the spot develops (see also table 2). This provides decisive evidence against the assumption of constant angles often made in three-dimensional transition modelling (e.g. Chen & Thyson 1971).

The data shown here suggest a measure of the 'strength' of the divergence in the flow. If we take the average angle of intersection between streamline and wedge boundary as approximately 12° on the inside and 3° on the outside of the bend, a little calculation shows that the angle between streamlines (at $x \simeq 400$ mm) is $\Delta\theta = 5$ deg. approximately. As the semi-angle of the wedge is $\alpha = 10°$ (and appears to be independent of curvature and divergence), an appropriate measure of the divergence is the flow angle ratio

$$\frac{\Delta\theta}{\alpha} = 0.5.$$

Indeed the configuration of the duct used in the present experiments was in part influenced by wanting a divergence ratio of order unity but not too small.

To study the celerities of the leading and trailing edges, the ensemble-averaged phase times ϕ_l, ϕ_t for the leading and trailing edges respectively are computed at each streamwise location at $\bar{z} = 0$, with results shown in figure 6 against $\bar{x}$. The figure indicates that, to an excellent approximation, ϕ_l, ϕ_t are linear and hence that the leading and trailing edge propagation velocities are constant, equal to $0.86U_\infty$ and $0.56U_\infty$ respectively, nearly the same as in two-dimensional flow (see table 2).

The variation of the propagation velocity at the spot boundaries for $y = 0.5$ mm is shown in figure 7 for three streamwise locations. Here the velocities are computed at different $\bar{z}$, and the variables are normalized appropriately with respect to free-stream velocity U_∞ and the distance $x - x_s$ measured from the spot source. If the spot structure were similar within the cone of propagation the distribution of the propagation velocities along $\bar{z}$ would collapse into a single curve with the above normalization. The corresponding distribution for two-dimensional flow reported by Wygnanski *et al.* (1976, hereafter referred to as WSF) is also superposed in figure 7 for comparison. It must be recalled that the WSF curve is a fit to their data at two

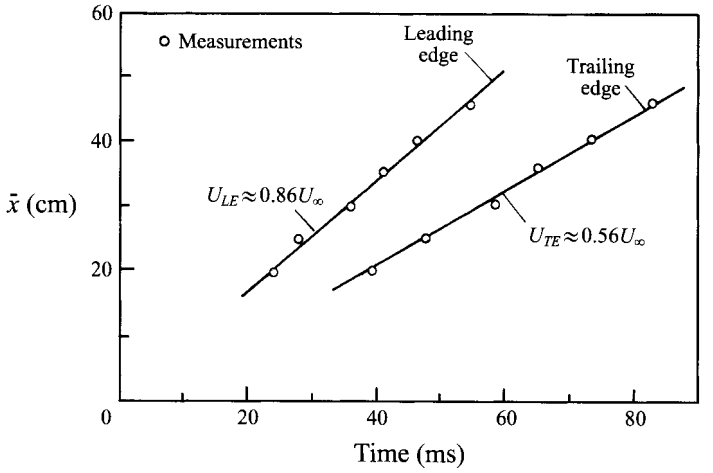

FIGURE 6. Celerity of leading and trailing edges of the spot at $y = 0.5$ mm (spot source located upstream of the bend).

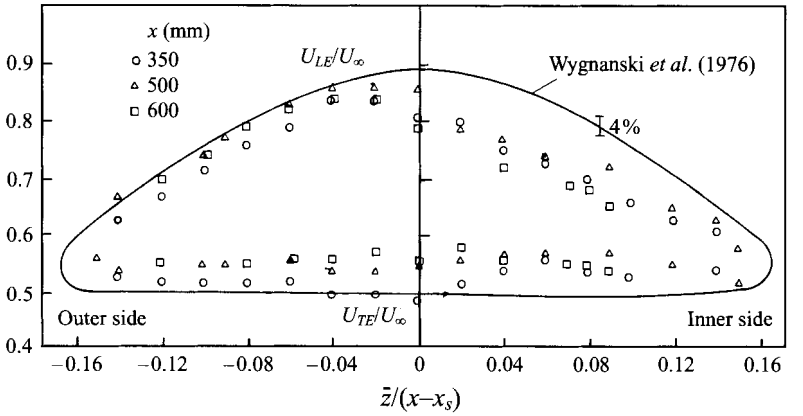

FIGURE 7. The spanwise variation of the propagation velocity at different streamwise locations for $y = 0.5$ mm.

heights, namely $y = 0.5$ and 5 mm, and that the scatter in their data amounts to about 4%.

On closer examination we see that the 'scatter' in figure 7 actually hides a systematic variation. In the first place, we find noticeable asymmetries in the present data between the 'inner' side (nearer the diverging sidewall) and the 'outer' side (nearer the flat sidewall): the leading edge of the spot travels faster on the outer side. However the trailing-edge propagation velocity is nearly constant for all $\bar{z}$. The lowest trailing-edge velocity at the centreline is seen at $x = 350$ mm, whereas the values are slightly higher at the wing tips at $x = 500$ and 600 mm. Further, on the inner side the celerities show no strong systematic variation, but on the outer side the (nearly constant) celerities at the two downstream stations ($x = 500$, 600 mm) are somewhat higher than at the first station ($x = 350$ mm). This suggests that the spot may be reaching a nearly invariant similarity state at $x = 500$ and 600 mm. In other words we may say that, even in this distorted flow, the spot propagation cone in x, t space (introduced by Emmons

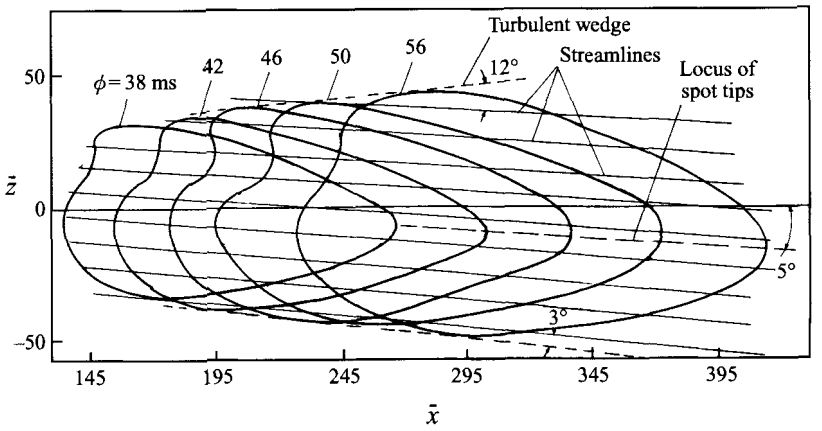

FIGURE 8. Plan view of evolution of a turbulent spot at $y = 0.5$ mm with time.

1951) eventually has straight generators, although its axis is not aligned with the local streamline.

4.1.2. *Spot shape*

The procedure adopted to find the spot shape is to determine the position at which the trailing and leading edges occur at a specified phase time ϕ, by linear interpolation or extrapolation (at extreme upstream and downstream stations, along streamlines in the streamwise direction, and along $\bar{z}$- and y-directions) from the data at the grid points shown in figure 5. The shape of the spot at a given ϕ is obtained by drawing a line passing through these leading and trailing edges.

Figure 8 shows the plan view of the section of the spot at the height $y = 0.5$ mm, as it develops in time, corresponding to $\phi = 38$, 42, 46, 50, 56 ms after the spot is generated. The streamlines in this region are also superposed in this figure for comparison. We are not aware of any earlier such measurements.

Although the spot possesses an arrow-head, it is not symmetrical about the centreline (bisector of turbulent wedge or $\bar{z} = 0$) of the spot envelope. The tip of the arrow-head seems to propagate along a streamline and not along the centreline, the angle between the two being about 5°. The spot spreads farther towards the outer side of the bend than it does towards the inner side, which is consistent with the celerities already indicated in figure 7. Clearly the spots have a distorted planform while maintaining a spread angle of the same value as in two-dimensional flows on a flat plate. Over the range of $\bar{x}$ over which an envelope can be drawn (about 190–290 mm), the angles of intersection with the local streamline are approximately 3° and 12°, in general agreement with the data of figure 5.

The normalized planform is shown in figure 9 at all the phase times. The normalization is made with length L_x of the spot along $\bar{z} = 0$ at $y = 0.5$ mm. Even though there is some scatter in the data shown, a mean shape can be clearly identified and is seen to differ appreciably from the normalized shape in two-dimensional flow, also shown in figure 9 for comparison (from the data of Schubauer & Klebanoff 1955). In particular, the sides of the distorted spot subtend very nearly the same angle of 31° as in two-dimensional flow (30.6° according to Schubauer & Klebanoff 1955).

Mean elevation views of the spot developing along $\bar{x}$, obtained by procedures similar to those described above, are shown in figure 10 for three spanwise stations corresponding to $\bar{z} = 30$, 0 and −30 mm. It is seen that spot cross-sections in

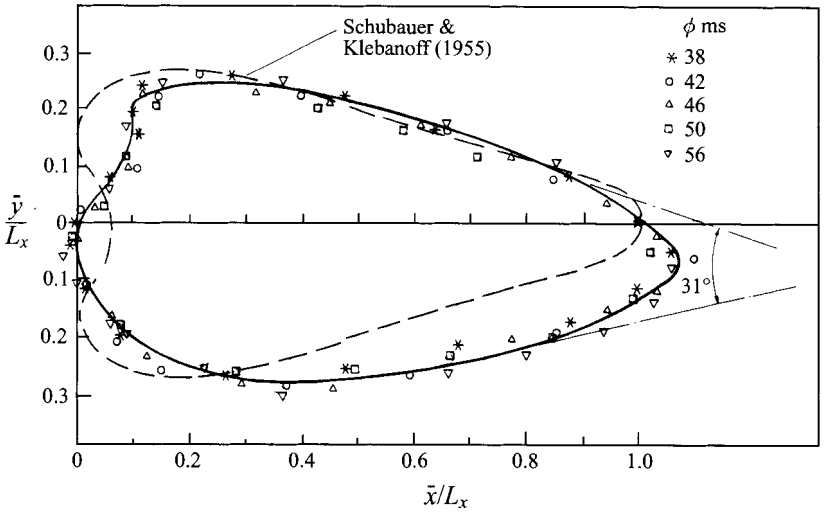

FIGURE 9. Normalized spot shape plan view at $y = 0.5$ mm and different time instants.

the vertical are approximately similar at each value of $\bar{z}$, but there is a measurable asymmetry and lack of similarity, hence construction of these shapes based on convection velocities and the conical growth assumption (used by WSF) would lead to error. The method adopted here depicts the true mean physical boundaries of the spot at the given phase time. The figure also shows the laminar boundary layer thickness, calculated from the approximate formula $\delta_L(x)/x \approx 5Re_x^{-1/2}$ assuming the origin to be at the leading-edge. The height of the overhang of the leading edge interface is slightly less than the thickness of the laminar boundary layer. It should be noted that the true laminar boundary layer thickness is likely to be slightly less than the local Blasius value if the divergence is taken into account (see Ramesh *et al.* 1993). A hypothetical turbulent boundary layer thickness (calculated from the approximate formula $\delta_L(x)/x \approx 0.37Re_x^{-1/5}$, Schlichting 1960), assuming that it originates at the spot source with an initial thickness equal to that of the laminar boundary layer, is also shown in the figure.

The elevations in figure 10 clearly show the normal hunch-back shape of the spot with an overhanging nose. However, the spot is thicker and has the longest overhang at $\bar{z} = -30$ mm. The speed of propagation of the nose, computed from two successive spot locations, is $0.99U_\infty$, suggesting convection at the free-stream velocity, as in two-dimensional flows. The tips of the overhang at $\bar{z} = 0$ and 30 mm travel slower than the free-stream velocity, namely at $0.9U_\infty$ and $0.86U_\infty$ respectively.

A normalized shape of the elevation of the spots is shown in figure 11 for the three spanwise locations. The normalization is carried out with respect to the length scale corresponding to the maximum length of the spot at a given $\bar{z}$, i.e. $L_{x1}(\bar{z})$ (distance from the point of the trailing edge on the plate to the projection of the overhanging tip on the surface, referring to figure 10). Once again the mean shape at each $\bar{z}$ is qualitatively similar. While points are scattered, specially at the top edge of the spot, it can be observed that the normalized shape is progressively getting squeezed at $\bar{z} = -30$ mm. The variation could be because the top of the spot may not grow exactly like a turbulent boundary layer. The variations seen in figure 11(a, c) must in part be due to the fact that the sections at $z = \pm 30$ mm do not correspond to a fixed value of the conical similarity variable. The elevation

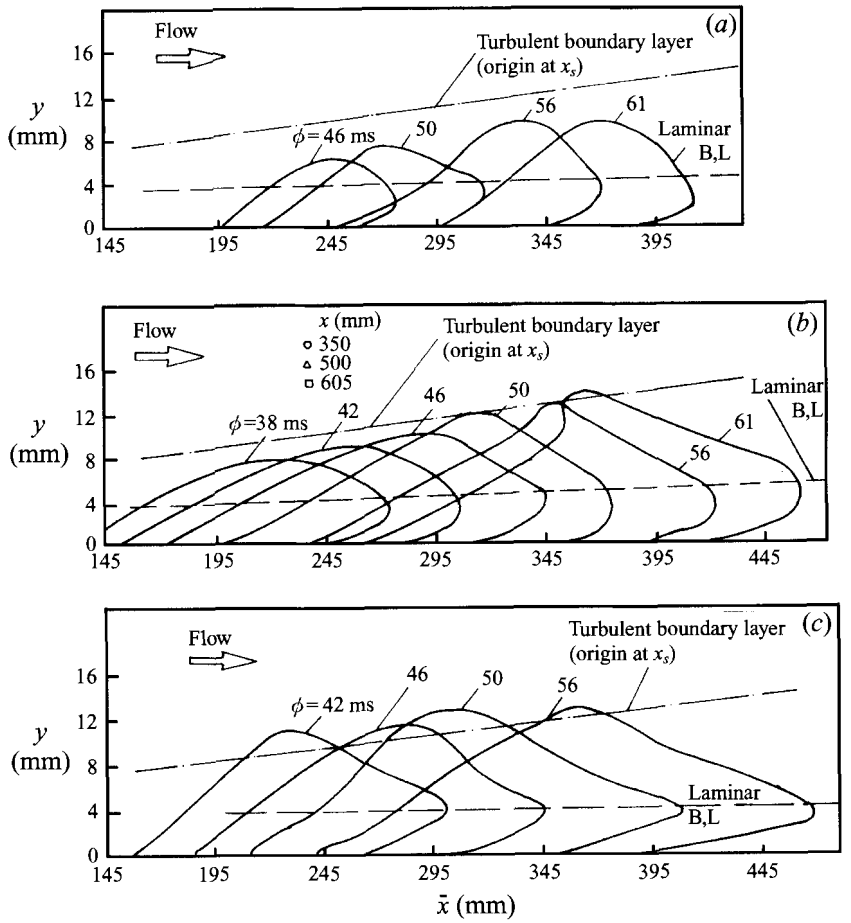

FIGURE 10. Elevation view of the development of the spot at different spanwise stations. (*a*) $z = 30$ mm, (*b*) $z = 0$, (*c*) $z = -30$ mm.

view of the spot in two-dimensional flow (traced by WSF) is also superimposed in figure 11(*b*) for comparison. Except at the top of the spot the shapes are in good agreement: the small differences that remain may in part be due to the different Reynolds numbers in WSF (508 and 1220, based on the laminar boundary layer displacement thickness at the spot source, compared to 450 in the present experiments).

Further examination shows that, compared to $\bar{z} = 0$, the spot has a relatively blunt nose near the overhang at $\bar{z} = 30$ mm and a relatively sharp nose near the overhang at $\bar{z} = -30$ mm. This may imply that the calm fluid around the spot entrained into it from the inner side of the bend tries to push the spot towards the straight wall, lifting the tip of the overhang further away from the surface. It could also be argued that fluid near the surface has lower velocity than away from it, and that this in turn produces progressively higher centrifugal force as one moves away from the wall surface; this eventually results in pushing the upper portion of the spot including the overhanging tip towards the outer side of the bend and hence produces the higher growth rate and stretched overhang observed at $\bar{z} = -30$ mm. This argument implies that the curvature of the spot trajectory has a strong influence on its structure.

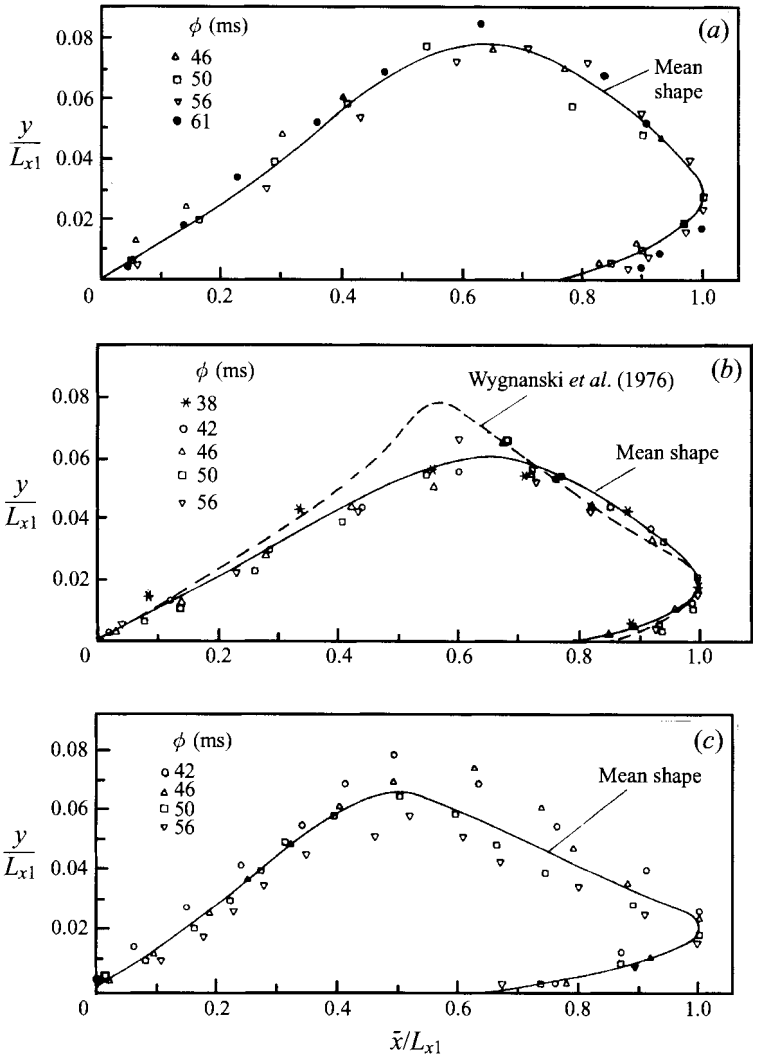

FIGURE 11. Normalized elevation view of the spot at different spanwise stations. (*a*) $z = 30$ mm, (*b*) $z = 0$, (*c*) $z = -30$ mm.

An obvious question raised by the present measurements is the reason for the observed asymmetry. If the kind of skewness seen in figure 11 is the result of streamline curvature as suggested above, it is at first sight somewhat surprising that this skewness not only does not disappear but even achieves some kind of similarity as the spot moves into a straight trajectory in the purely divergent part of the duct. The surprise is enhanced by the fact that the flow asymptotically corresponds to a first approximation to radial flow from a source far upstream, as may be inferred from figure 5; and this inference is supported by detailed analysis (Ramesh *et al.* 1993). However, the flow even in the purely divergent part of the duct is not symmetrical, because of the transverse gradient in the boundary layer thickness, as demonstrated in figure 4. The contribution from this residual asymmetry in the background flow was estimated from the subsidiary series of experiments. The results are discussed in §4.5 and summarized in table 2.

4.2. *Phase-averaged velocity time traces*

Mean velocity characteristics of the spot are obtained by taking ensemble averages at each phase with respect to the leading edge as reference point as this is less ambiguous than the trailing edge.

Figure 12 shows the phase-averaged velocity distribution thus obtained in the spot as a function of time for different distances from the wall at various spanwise stations. Note that in figure 12 time is still counted from the trigger generating the spot and not from the leading edge, enabling us to study the variation of the arrival time of the leading edge with height from the wall. As an example, the mean leading- and trailing-edge phase times are marked in figure 12(*b*) to depict their variation with distance from the wall. A careful observation of this figure shows that the leading edge arrives earlier as y increases up to $y = 4$ mm, beyond which the arrival is delayed. This is essentially the effect of the overhang of the spot. The main quantitative features of the phase-averaged velocity distribution are similar to those measured in two-dimensional spots, e.g. WSF, Van Atta & Helland (1980), Antonia *et al.* (1981), Itsweire & Van Atta (1984), Gostelow *et al.* (1992). Thus, near the wall the velocity increases sharply as the spot passes the measuring point and leaves behind a wake which slowly decelerates and attains the undisturbed laminar boundary layer velocity at that height from the surface. Towards the outer edge of the spot the velocity decreases as the spot moves past the measurement point and in the wake the velocity accelerates to the undisturbed velocity. Around the overhanging tip the speed decreases first and then accelerates later to leave a wake which again decelerates to the undisturbed flow in the laminar boundary layer.

From this figure we can plot the time duration of spot passage as a function of y at a fixed streamwise position for each value of $\bar{z}$ (figure 13). This time duration is larger at $\bar{z} = 0$ and -30 mm than at $\bar{z} = 30$ mm near the wall and will be almost same at the outer edge of the spot boundary (at $y = 30$ mm).

Another important feature of the velocity traces is the emergence of Tollmien–Schlichting waves of the type observed in two-dimensional flows and studied in some detail by Wygnanski *et al.* (1979). What is striking in the present data is that the waves, observed off the centre of the turbulent wedge, are much stronger at $\bar{z} = -30$ mm (see figure 12*c*) than at $\bar{z} = 30$ mm. Clearly the destabilization of the flow is much weaker on the inner side of the bend in the present flow. This asymmetry is consistent with the observations reported in §4.1, indicating that the spots are squeezed on the inside (see figure 13*a*) since it takes longer for Tollmien–Schlichting waves to develop. A possible reason for the weaker waves at the inner wing tip is that the boundary layer Reynolds number is lower on the inside.

Our observations also show occasional breakdown of these waves downstream (chiefly on the outer side of the bend), leading to the birth of what may be called spotlets, as reported by Wygnanski *et al.* (1979); once again however the breakdowns are more frequent on the outside of the bend. A detailed investigation of this matter is outside the scope of the present paper.

4.3. *Mean flow field inside turbulent spot*

Conditional time averages (taken during passage of the spot only, and eliminating the non-turbulent regions), are not very illuminating for understanding the structure of a turbulent spot because of the relatively high variability from spot to spot, but are of great interest in transition zone modelling (e.g. Narasimha 1985). Figure 14 shows a log-log plot of such average velocity profiles inside a spot at three spanwise stations

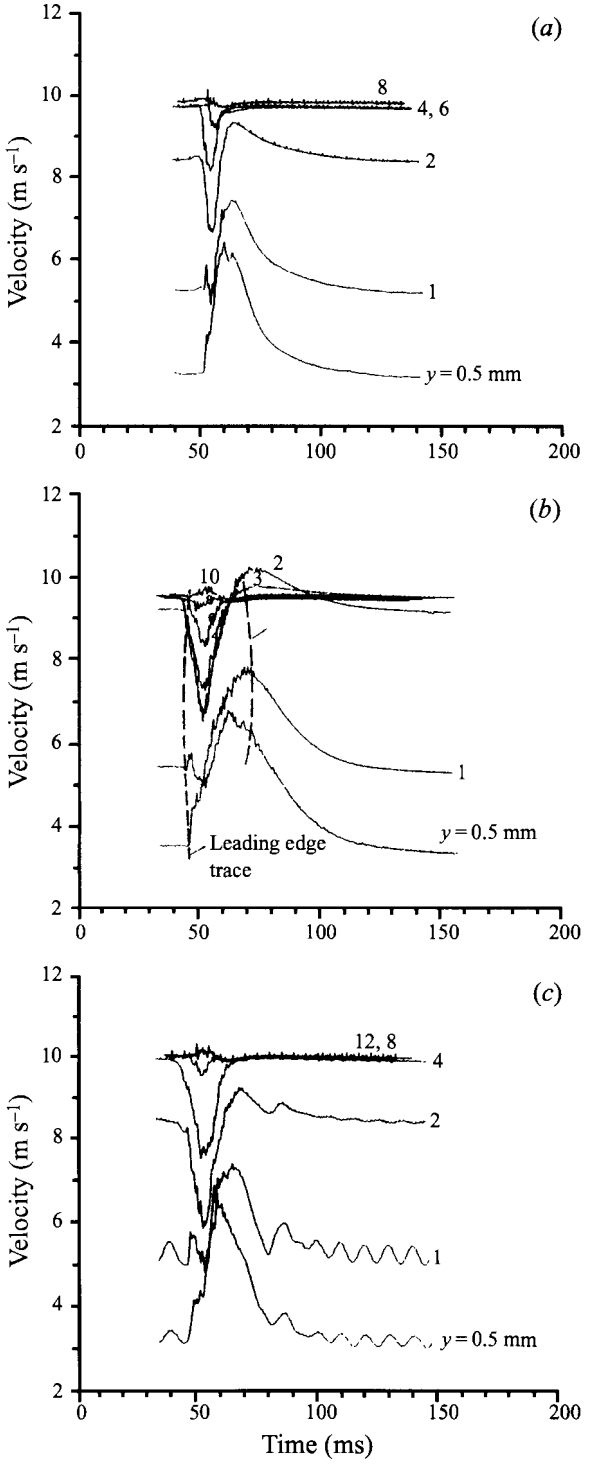

FIGURE 12. Time trace of phase-average velocity signal at various distances from the wall at $x = 450$ mm and different spanwise stations. (*a*) $\bar{z} = 30$ mm, (*b*) $\bar{z} = 0$, (*c*) $\bar{z} = -30$ mm.

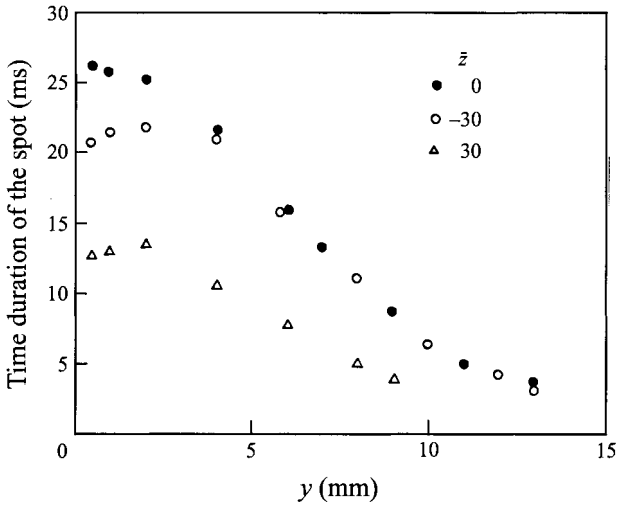

FIGURE 13. Variation of time duration of the spot in the y-direction at different spanwise stations.

($\bar{z} = 0$, 30 and -30 mm) at $x = 500$ mm. All these curves are non-dimensionalized with respect to free-stream velocity and a thickness defined by the $0.99U_\infty$ point. Because the elevation of the spot varies in the spanwise direction, it is perhaps not surprising that conditional velocity profiles do not collapse onto a single curve. It can be seen that they follow power laws (i.e. $u/U_\infty = (y/\delta)^{1/n}$) with different values for the exponent, namely $n = 3.7$, 4.3, and 5.9 for $\bar{z} = 30$, -30, and 0 mm respectively; it has recently been argued by Barenblatt (1992) that such power laws could be a valid method of analysis.

To determine exactly which regions within the spot obey the universal log law, typical velocity profiles (at $\bar{z} = 0$, $x = 500$ mm) deduced from ensemble-averaged data are shown on a semi-log plot in figure 15. We observe that only the 53 ms profile exhibits a linear region. However, a zonally averaged (see §3) velocity profile (essentially an average over the whole spot) does exhibit logarithmic velocity variation (figure 14) as in a fully turbulent profile. Unfortunately the measurements made here did not include the local wall stress, so we cannot assert the universality of the constants in the log profile. Nevertheless it seems that the construction of a synthetic transition profile, combining a turbulent profile when the spot occurs with a laminar profile when the spot is not there, is likely to be meaningful even in diverging flows.

4.4. *Perturbation flow field*

The perturbation flow fields of the spot are obtained by subtracting the steady longitudinal velocity of the unperturbed laminar boundary layer from the ensemble-averaged velocity within the spot. A typical contour plot of the perturbation velocity field in planform view, along with the measured boundary of the turbulent spot, is shown in figure 16. The inner structure of the spot shows a small region of velocity excess just downstream of the trailing edge. Note the presence of peaks amd valleys in the central region of the spot, consistent with a pair of counter-rotating vortices which entrain fluid from the laminar flow outside the spot, and the appearance of Tollmien–Schlichting (T-S) waves at the wing tips, specially on the outer side of the bend.

The elevation views of the perturbation velocity field are shown in figure 17. The corresponding height and length of the spot at a fixed phase time at $y = 0.5$ mm are

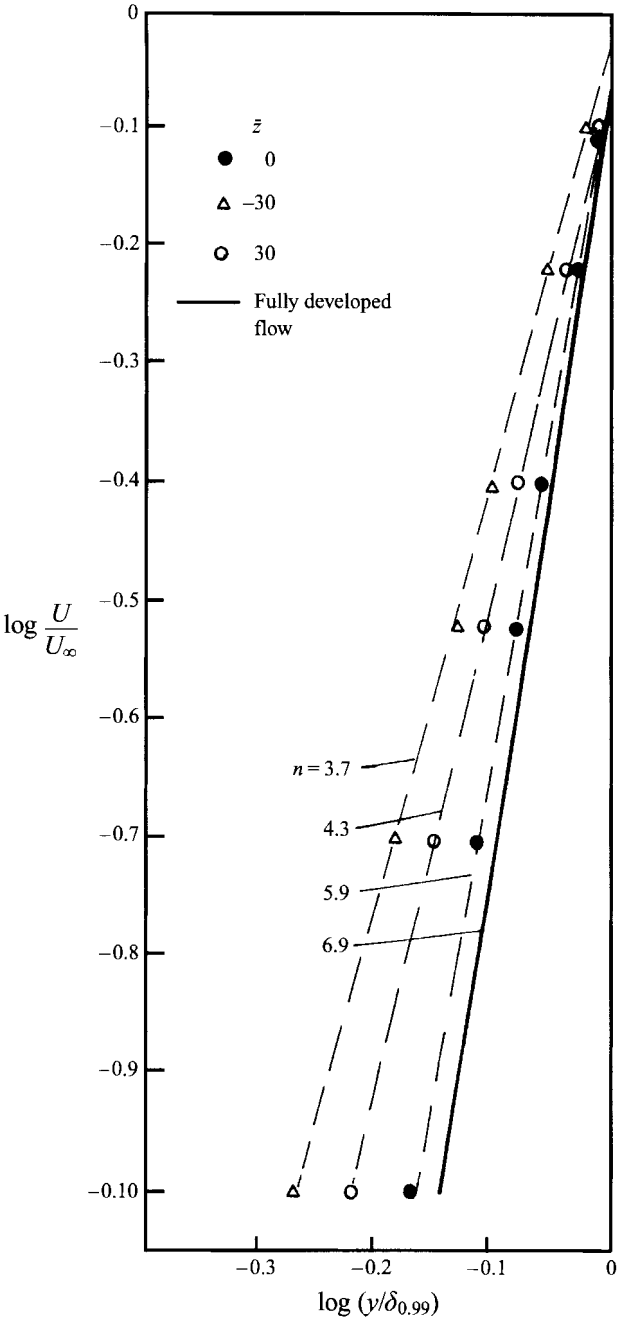

FIGURE 14. Log-log plot of velocity profiles within the spot at different spanwise stations and $x = 500$ mm.

used for non-dimensionalizing the y and $\bar{x}$ coordinates respectively. Here again, as in the plan views, the values of velocity perturbation are indicated as a percentage of free-stream velocity. In this figure the spot is represented by a closed loop of velocity defect extending outward from y/spot height = 0.1, riding above the contours representing excess velocity, which also trail behind the turbulent region.

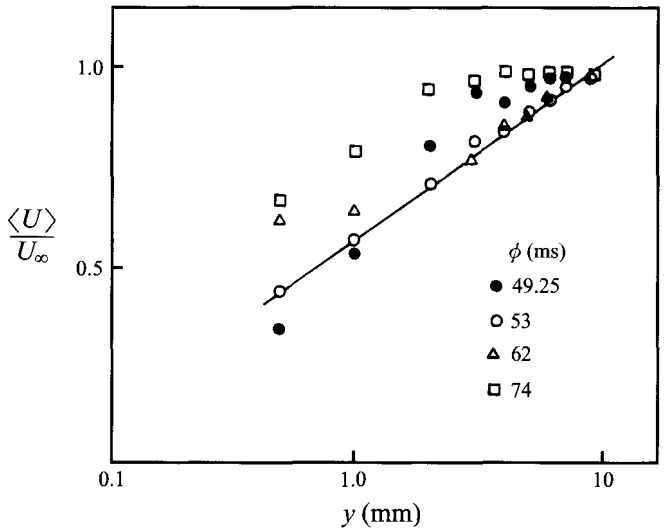

FIGURE 15. Semi-log plot of velocity profiles at different time intervals through the spot for $z = 0$ and $x = 500$ mm.

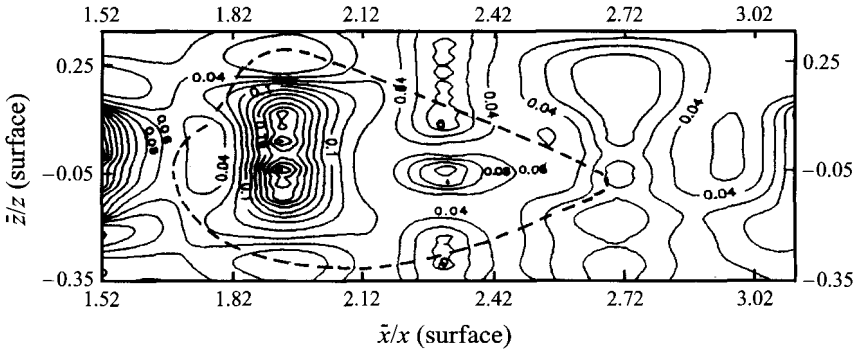

FIGURE 16. Contour plot of perturbed velocity field at 42 ms in normalized (x, z)-plane for $y = 0.5$ mm.

Since the excess velocity decays rather slowly behind the spot, the trailing interface near the wall does not follow any contour of constant velocity perturbation. The widely separated contours in this figure above or ahead of the active turbulent region, representing a slight velocity defect, may be related to the calm region left behind by the preceding spot.

Figure 17 is quite similar to those of Zilberman, Wygnanskik & Kaplan (1977), Antonia *et al.* (1981) and Itsweire & Van Atta (1984) except that due to the streamline divergence the present contours are distorted and the conventional overhang and slanted trailing edge shapes are sometimes difficult to distinguish. This leads us to the important conclusion that the chief effect of distortion on the spot structure is *geometrical* rather than *dynamical*; i.e. there is no dramatic difference in the structure of the spot itself, but the parameters that describe it display quantitative differences because of the distortion.

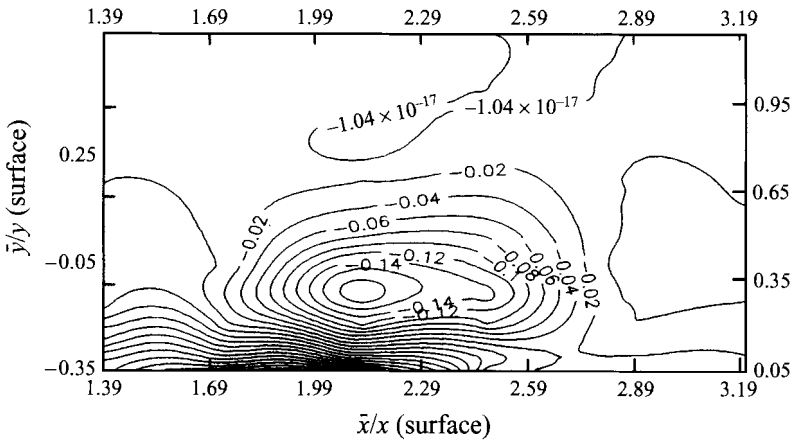

FIGURE 17. Contour plot of perturbed velocity field at 46 ms in normalized (x, y)-plane for $z = 0$. (Topmost contour represents machine zero on computer.)

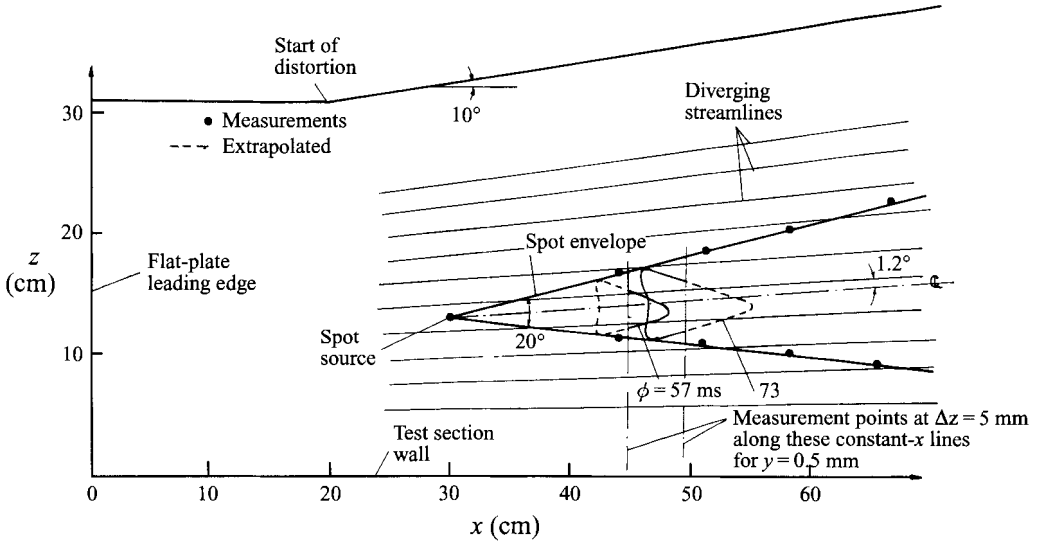

FIGURE 18. Spot envelope at $y = 0.5$ mm from the plate in subsidiary series of experiments (spot source located downstream of the bend).

4.5. *Divergence vs. curvature*

The most striking feature of the distorted spot studied here is its lateral asymmetry, which can be attributed to (*a*) curvature of the streamlines at the entry of the distorted duct and/or (*b*) the distortion already present in the development of the laminar boundary layer into which the spot propagates. In order to throw some light on these effects preliminary experiments were conducted in the subsidiary series (at a wind speed of 6.2 m s^{-1}, spot generation frequency reduced to 1 Hz), with the spot source located downstream of the bend (see figure 18) in the diverging section with straight streamlines, thus avoiding the direct effect of curvature.

Measurements were carried out at two streamwise stations, namely $x = 450$ and 500 mm, and at each of these stations data were collected along the z-direction at an

interval of 5 mm to cover the whole region of the spot envelope. Beyond $x = 600$ mm it was observed that, due to the strong amplification of the T-S waves and occurrence of natural transition, the spots cannot be distinguished from the background flow.

From figure 18, the spot envelope from this subsidiary set of measurements is seen to be a single wedge starting from the spot source, the angle of this wedge being again 20°, in excellent agreement with the previous set of measurements (see figure 5). Unlike the earlier results there is no reorientation of the wedge in the distorted duct, and the virtual origin of the wedge coincides with the spot source itself. However, from the local streamlines superimposed on the spot envelope, we see that the centreline of the wedge is not along any streamline, although the angle (1.2°) is rather lower than that in the earlier measurements (3.5°). This suggests that streamline curvature and divergence both have comparable effects on spot propagation. Further, the angle that the wedge boundary makes with the local streamlines (see table 2) is still different on the two sides and changes as the spot develops, confirming again that the intersection angles are not unique, although the variations now are somewhat smaller.

The plan views of the spot as it develops in time, corresponding to phase times $\phi = 57$ and 73 ms (after the spot is generated), are shown in figure 18. The spot shapes found here resemble more closely the conventional two-dimensional spots with an arrow-head nose; however like previous results (see figure 8) the tip of the arrow-head propagates along a streamline and not along the centreline of the turbulent wedge, and spreads farther towards the outer side of the bend than it does towards the inner side. This result confirms that asymmetry in the flow influences the spot characteristics even in the absence of the curvature effect.

Further evidence of the distortion of the spot is provided by the appearance of T-S waves trailing the spot on the outer side of the bend, as shown in figure 19. This figure shows the velocity traces at the downstream station ($x = 500$ mm), for different spanwise locations, namely, $z = 135$, 140, 155 and 160 mm. Looking at this figure it is quite clear that, as one moves away from the inner side of the bend, say at $z = 160$ mm, towards the outer side, say $z = 135$ mm, T-S waves appear adjacent to the spot boundary and are stronger at the downstream stations. So the fact that these waves, which are related to the spot shape and its spread, amplify more strongly on the outer side of the bend is further evidence of the deviation of the spot from symmetry due to streamline divergence.

The only explanation for the distortion of the spot in the subsidiary series of experiments appears to be the distortion of the laminar boundary layer into which the spot propagates. We have already seen (figure 4) that the boundary layer thickness increases linearly from the inner side of the bend towards the outer side, and that this increment is more pronounced at the downstream stations, e.g. $x = 600$ mm. We conclude that the spot generated downstream of the bend is influenced solely by this distortion in the laminar boundary layer and hence gets tilted towards the outer side of the bend where the boundary layer is thicker.

On the other hand, as in §4.1, it is found that the celerities agree closely with the values obtained in the main series of experiments and hence also with those in two-dimensional flows (see table 2).

5. Conclusions

The main outcome of the present study is the following set of results.

1. Overall spot characteristics like the spread angle and the celerity of the leading and trailing edges do not depend strongly on streamline divergence or curvature,

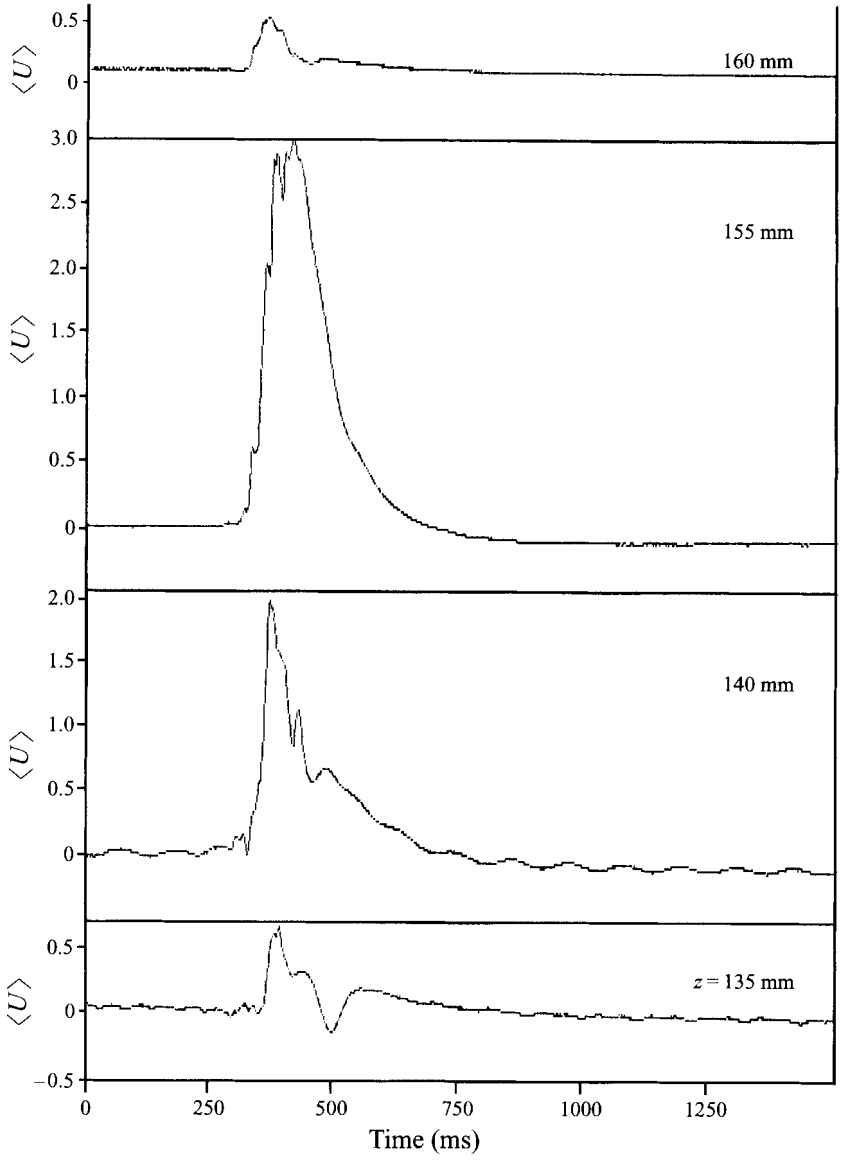

FIGURE 19. Conditionally averaged velocity time traces at $x = 500$ mm along spanwise direction, in subsidiary series of experiments.

even when the divergence (i.e. change in flow angle across the spot) is of the order of the spot growth angle and the spot shape is distorted. The spot propagation across streamlines, however, is not at a constant angle as in two-dimensional flows: it varies from 13° to 10° on the inner side of the bend to 3° on the outer side in the present study (in the main series of experiments), and contradicts an assumption frequently made in models for the transition zone.

2. The plan view of the spots shows that the tip of the spot does not propagate along the axis of the wedge that forms the envelope of spot positions but moves outward at an angle of 5°. The spots have substantially distorted planforms but these nevertheless exhibit similarity at different time instants. This implies that the

spot retains a certain universality while propagating downstream, in spite of the fact that the transverse curvature that must be one principal reason for the asymmetry is absent at stations further downstream.

3. Normal cross-sections of the spot on planes parallel to the bisector of the turbulent wedge resemble those of a spot in two-dimensional flow. The effect of the distortion is to elongate the overhanging tip of the spot on the outer side of the bend and shorten it on the inner side. These spot cross-sections do not show any self-similarity, the departures from similarity being largest near the leading edge and around the overhanging tip.

4. Phase-averaged velocity-time variations show characteristics similar to those of two-dimensional flow reported in the literature.

5. Velocity traces reveal Tollmien–Schlichting waves trailing the spot near the wall as in two-dimensional flow, but they are more pronounced on the outer side.

6. The phase-averaged mean velocity profiles within the spot follow power laws, however, with exponents varying from 3.7 to 5.9 in the spanwise direction at $x =$ 500 mm. They do not individually show the standard logarithmic behaviour but the *global* mean within the spot does so. This supports the construction of intermittency-weighted mean velocity profiles in transition zone models.

7. The flow fields associated with the passage of the spot, displayed as contour plots of the velocity perturbation, are consistent with a pair of counter-rotating vortices which entrain fluid from the surrounding laminar flow, and show that the eddies and their propagation in the downstream direction are similar to those in two-dimensional flows. These observations suggest that transverse curvature and flow divergence, at the levels studied here, produce chiefly a *geometric* distortion of the coherent structure in the spot, without affecting the dynamics in any substantial way.

This project was supported by Department of Science and Technology, Government of India. The authors wish to thank Mr Phani Kumar for his assistance in conducting the experiments.

REFERENCES

AHMED, A., WENTZ, W. H., & NYENHUIS, R. 1989 *J. Aircraft* **26**, 979–985.

ANTONIA, R. A., CHAMBERS, A. J., SOKOLOV, M. & VAN ATTA, C. W. 1981 *J. Fluid Mech.* **108**, 317–343.

ARNAL, D. & JUILLEN, J. C. 1977 *Recherche Aerospatiale* **1977–2**, 147–166.

BARENBLATT, G. I. 1992 *J. Fluid Mech.* **248**, 513–520.

CANTWELL, B., COLES, D. & DIMOTAKIS, P. 1978 *J. Fluid Mech.* **87**, 641–672.

CHAMBERS, F. W. & THOMAS, A. S. W. 1983 *Phys. Fluids,* **26**, 1160–1162.

CHEN, K. K. & THYSON, N. A. 1971 *AIAA J.* **9**, 821–825.

CLARK, J. P., JONES, T. V. & LAGRAFFE, J. E. 1993 *J. Engng Maths* **28**, 1–19.

COLES, D. E. 1981 *Proc. Ind. Acad. Sci.* (ES) **4**, 111–127.

EMMONS, H. W. 1951 *J. Aero. Sci.* **18**, 490–498.

EMMONS, H. W. & BRYSON, A. E. 1952 *Proc. 1st US Natl Congr. on Appl. Mech.*, pp. 852–868.

GAD-EL-HAK, M., BLACKWELDER, R. F. & RILEY, J. J. 1981 *J. Fluid Mech.* **110**, 73–95.

GOSTELOW, J. P. & BLUNDEN, A. R. 1992 *Proc. ASME Gas Turbine Conference, Cologne, June 1992.*

GOSTELOW, J. P., HONG, H. & SHEPPEARD, M. A. 1992 *Proc. ISROMAC 4 Honolulu, Hawaii.*

GUTMARK, E. & BLACKWELDER, R. F. 1987 *Exps. Fluids* **5**, 217–229.

HEDLEY, T. B. & KEFFER, J. F. 1974. *J. Fluid Mech.* **64**, 625–644.

ITSWEIRE, E. C. & VAN ATTA, C. W. 1984 *J Fluid Mech.* **148**, 319–348.

JAHANMIRI, M., PRABHU, A. & NARASIMHA, R. 1995 *Laminar-Turbulent Transition, Proc. IUTAM Symp., Sendai, Japan Sept. 1994* (ed. R. Kobayashi). Springer.

JAHANMIRI, M., RUDRA KUMAR S. & PRABHU, A. 1991 *Fluid. Mech. Rep.* 91 FM 13. Dept. Aero. Engng., Ind. Inst. Sci. Bangalore.

KATZ, Y., SEIFERT, A. & WYGNANSKI, I. 1990 *J. Fluid Mech.* **221**, 1–22.

KOHAMA, Y. 1988 In *Turbulence Management and Relaminarization, Proc. IUTAM Symp., Bangalore 1987* (ed. H. W. Liepmann & R. Narasimha). Springer, Berlin.

KOVASZNAY, L. S. G., KIBENS, V. & BLACKWELDER, R. F. 1970 *J. Fluid Mech.* **41**, 283–325.

KOWSKY, P. N. & BIPPES, H. 1988 *Phys. Fluids.* **31**, 786–795.

KUAN, C. L. & WANG, T. 1990 *Expl Therm. Fluid. Sci.* **3**, 157–173.

NARASIMHA, R. 1985 *Prog. Aero. Sci.* **22**, 29–80.

NARASIMHA, R., DEVASIA, K. J., GURURANI, G. & BADRINARAYANAN, M. A. 1984*a* *Exps. Fluids* **2**, 171–176.

NARASIMHA, R., SUBRAMANIAN, C. & BADRINARAYANAN, M. A. 1984*b* *AIAA J.* **22**, 837–839.

PERRY, A. E., LIM, T. T. & TEH, E. W. 1981 *J. Fluid Mech.* **104**, 387–407.

POLL, D. I. A. 1985 *J. Fluid Mech.* **150**, 329–356.

PRABHU, A. & RAO, B. N. S. 1981 *Fluid Mech. Rep.* 81 FM 10. Dept. Aero. Engng, Ind. Inst. Sci., Bangalore.

RAMESH, O. N., DEY, J. & PRABHU, A. 1993 *AIAA J.* **32**, 209–210.

RILEY, J. J. & GAD-EL-HAK, M. 1985 The dynamics of turbulent spots. In *Frontiers in Fluid Mechanics* (ed. S. H. Davis & J. L. Lumley), pp. 123–155. Springer.

SADDOUGHI, S. G. & JOUBERT P. N. 1991 *J. Fluid Mech.* **229**, 173–204.

SCHLICHTING, H. 1960 *Boundary Layer Theory.* McGraw Hill.

SCHUBAUER, G. B. & KLEBANOFF, P. S. 1955 *NACA Tech. Note* 3489.

SMITH, F. T. 1994 (ed.) *J. Engng Maths* **28**, 1–91.

VAN ATTA, C. W. & HELLAND, K. N. 1980 *J. Fluid Mech.* **100**, 243–255.

WYGNANSKI, I. 1981 In *The Role of Coherent Structures in Modelling Turbulence and Mixing, Proc. Intl Conf. Madrid 1980* (ed. J. Jimenez). Springer.

WYGNANSKI, I., HARITONIDIS, J. H. & KAPLAN, R. E. 1979 *J. Fluid Mech.* **92**, 505–528.

WYGNANSKI, I., SOKOLOV, M. & FRIEDMAN, D. 1976 *J. Fluid Mech.* **78**, 785–819 (referred to herein as WSF).

WYGNANSKI, I., ZILBERMAN, M. & HARITONIDIS, J. H. 1982 *J. Fluid Mech.* **123**, 69–90.

ZILBERMAN, M., WYGNANSKI, I. & KAPLAN, R. E. 1977 *Phys. Fluids Suppl.* **20**, S258–S271.